

New H₂O masers in Seyfert and FIR bright galaxies II. The intermediate luminosity range[★]

P. Castangia^{1,2}, A. Tarchi^{2,3}, C. Henkel¹, and K. M. Menten¹

¹ Max-Planck-Institut für Radioastronomie, Auf dem Hügel 69, 53121 Bonn, Germany
e-mail: pcastang@mpi.fr-bonn.mpg.de

² INAF – Osservatorio Astronomico di Cagliari, Loc. Poggio dei Pini, Strada 54, 09012 Capoterra (CA), Italy

³ INAF – Istituto di Radioastronomia, via Gobetti 101, 40129 Bologna, Italy

Received 19 July 2007 / Accepted 28 November 2007

ABSTRACT

Context. Recently, a relationship between the water maser detection rate and far infrared (FIR) flux density has been found as a result of a 22 GHz maser survey in a sample comprised of northern galaxies with 100 μm flux density $>50 \text{ Jy}$ and a declination $>-30^\circ$.

Aims. The survey has been extended toward galaxies with lower FIR flux densities in order to confirm this correlation and to discover additional maser sources for relevant follow-up interferometric studies.

Methods. A sample of 41 galaxies with $30 \text{ Jy} < S_{100\mu\text{m}} < 50 \text{ Jy}$ and $\delta > -30^\circ$ was observed with the 100-m telescope at Effelsberg in a search for the 22 GHz water vapor line. The average 3σ noise level of the survey is 40 mJy for a 1 km s^{-1} channel, corresponding to a detection threshold for the isotropic maser luminosity of $\sim 0.5 L_\odot$ at a distance of 25 Mpc.

Results. Two detections are reported: a megamaser with an isotropic luminosity, $L_{\text{H}_2\text{O}}$, of $\approx 35 L_\odot$ in the Seyfert/HII galaxy NGC 613 and a kilomaser with $L_{\text{H}_2\text{O}} \approx 1 L_\odot$ in the merger system NGC 520. The high luminosity and the presence of a Seyfert nucleus favor an association for NGC 613 with an active galactic nucleus. The kilomaser in NGC 520 was also detected with the Very Large Array, providing a position with subarcsecond accuracy. The H₂O emission, originating from a $\lesssim 0.02 \text{ pc}$ sized region with a brightness temperature $\gtrsim 10^{10} \text{ K}$ (if the observed variations are intrinsic to the masing cloud(s)), is close to one of the two radio continuum sources located in the inner parsecs of NGC 520. The maser is most likely associated with a young supernova remnant (SNR), although an association with a low-luminosity AGN (LLAGN) cannot be ruled out. The maser detection rate, with 2 new maser sources out of 41 galaxies observed, is consistent with expectations extrapolated from the statistical properties of the $S_{100\mu\text{m}} > 50 \text{ Jy}$ sample. The H₂O kilomasers are “subluminous”, while H₂O megamasers tend to be “superluminous” with respect to the FIR luminosity of their parent galaxy, when compared with sites of massive star formation in the Milky Way.

Key words. masers – galaxies: active – galaxies: nuclei – galaxies: starburst – galaxies: statistics – radio lines: galaxies

1. Introduction

Water maser emission at 22 GHz ($\lambda \sim 1.3 \text{ cm}$) originates from the transition between the 6_{16} and 5_{23} rotational levels of ortho-H₂O and forms in dense ($n(\text{H}_2) \gtrsim 10^7 \text{ cm}^{-3}$) and warm ($T_{\text{kin}} \gtrsim 400 \text{ K}$) molecular gas (Henkel et al. 2005a). The most plausible inversion mechanism is collisional pumping with H₂ molecules (Neufeld et al. 1994). In the Galaxy, water maser sources are common in regions of star formation and in the circumstellar envelopes of mass-losing oxygen-rich evolved stars. Since 1977, when the first extragalactic maser was detected in the nearby spiral galaxy M 33 (Churchwell et al. 1977), this maser line has been observed in ~ 100 external galaxies (Braatz 2007, priv. com.). Isotropic 22 GHz line luminosities of extragalactic H₂O masers, $L_{\text{H}_2\text{O}}$, range from $10^{-2} L_\odot$ (e.g., M 33, Churchwell et al. 1977; IC 10, Henkel et al. 1986; IC 342, Tarchi et al. 2002b) to $23\,000 L_\odot$ (SDSS J0804+3607, Barvainis & Antonucci 2005); for a review see Lo (2005).

The luminous extragalactic masers, with $L_{\text{H}_2\text{O}} > 10 L_\odot$, are classified as “megamasers” and are mostly found in galaxies with Seyfert 2 or LINER characteristics, exhibiting very high X-ray absorbing column densities ($N_{\text{H}} > 10^{23} \text{ cm}^{-2}$;

Zhang et al. 2006). So far, Very Long Baseline Interferometry (VLBI) studies have been reported for about 10 megamaser sources and all indicate that the maser emission is located within a few parsecs from the associated active galactic nucleus (AGN), being related to (1) nuclear accretion disks (e.g., NGC 4258, Greenhill et al. 1995; Miyoshi et al. 1995; IC 2560, Ishihara et al. 2001; Mrk 1419, Henkel et al. 2002) (2) interactions between the jet(s) emerging from the nucleus and ambient molecular clouds (e.g., NGC 1052, Claussen et al. 1998; NGC 1068, Gallimore et al. 2001; Mrk 348, Peck et al. 2003), and (3) nuclear outflows (Circinus, Greenhill et al. 2003a).

The less luminous extragalactic masers, the so-called “kilomasers”, with $L_{\text{H}_2\text{O}} < 10 L_\odot$, are usually found in star-forming galaxies and the majority of them are associated with star-forming regions clearly offset from the nucleus (e.g., M 33, Churchwell et al. 1977; M 82, Baudry & Brouillet 1996; IC 10, Henkel et al. 1986; IC 342, Tarchi et al. 2002b; NGC 2146, Tarchi et al. 2002a). However, in 3 galaxies, M 51 (Hagiwara et al. 2001), NGC 4051 (Hagiwara et al. 2003), and NGC 253 (Henkel et al. 2004), kilomaser emission is also arising from the nuclear region, with projected distances from the putative nucleus of <15 , 5, and 6 pc, respectively. Among these, only the kilomaser in M 51 has been definitely associated with an AGN, most likely with the radio jet (Hagiwara 2007). Instead,

[★] Based on observations with the 100-m telescope of the MPIfR (Max-Planck-Institut für Radioastronomie) at Effelsberg.

the kilomaser in NGC 253 turned out to be associated with a supernova remnant in the proximity of the nucleus (Hofner et al. 2006). The nature of the water maser emission in NGC 4051 is still uncertain and needs to be investigated at higher resolution (Hagiwara 2007). The possibility that some kilomasers could be related to nuclear activity (like M 51 and, possibly NGC 4051), similarly to the more powerful megamasers, is exciting and would provide a new tool for studying their host galaxies' nuclear regions. Hence, given the small number (15) of kilomasers found so far, this motivates extended searches to find more of these sources.

The sample: Searching for 22 GHz water vapor masers toward a sample comprised of all galaxies with declination $\delta > -30^\circ$ and $100\mu\text{m}$ IRAS point source flux densities $S_{100\mu\text{m}} > 50\text{Jy}$, led to four new detections (Tarchi et al. 2002a,b; Henkel et al. 2005b, hereafter HPT), yielding a total detection rate of 22%. A relationship between FIR flux density and likelihood of detectable water maser emission was also established. Motivated by these results, we have decided to extend the observational campaign toward lower infrared fluxes, to confirm the correlation found and to discover additional maser sources suitable for interferometric follow-up observations. The sample includes all galaxies with $\delta > -30^\circ$ and IRAS point source flux densities $30\text{Jy} < S_{100\mu\text{m}} < 50\text{Jy}$ with known recessional velocities. The list of sources, shown in Table 1, was compiled using the IRAS Point Source Catalog (Fullmer & Lonsdale 1989). For three of the 41 target galaxies listed, NGC 613 (Henkel et al. 1984; Braatz et al. 1996), NGC 5135 (Braatz et al. 2004), and NGC 6951 (Claussen & Lo 1986; Braatz et al. 1996, 2004) upper limits had already been determined. Because of the time variability of the 22 GHz H₂O maser emission, the sources were re-observed. In the following, we describe the results of this new survey.

2. Observations and data reduction

2.1. Effelsberg observations

Measurements in the $6_{16}-5_{23}$ transition of ortho-H₂O (rest frequency 22.23508 GHz) were carried out with the MPIfR 100-m telescope at Effelsberg¹, Germany, between April 2004 and November 2005. The full width to half power (FWHP) beamwidth was $\approx 40''$ and the pointing accuracy was, on average, $4''$ and always better than $20''$. Throughout the survey, we used a *K*-band high electron mobility transistor (HEMT) receiver with two orthogonally linearly polarized channels and a rotating feed that was switched between two fixed position separated by $\sim 2'$ at a frequency of 1 Hz. The spectrometer was an 8192 channel correlator (AK 90) in which the signal was split into 8 bands (IFs) of width 40 MHz and 512 channels each, yielding a channel spacing of $\sim 78\text{ kHz}$ ($\sim 1.04\text{ km s}^{-1}$). Four intermediate frequency bands (“IFs”) were centered at a frequency corresponding to the local standard of rest (LSR, optical convention) recessional velocity of each galaxy, while the others had frequency offsets of $\pm 20\text{ MHz}$. On January 21, 2005 we also took a high spectral resolution spectrum of NGC 520 using 2 bands of 20 MHz and 4096 channels each, yielding a spacing of $\sim 5\text{ kHz}$ (0.07 km s^{-1}).

To establish a flux density scale, the continuum sources NGC 7027, 3C 286, and W3(OH) were observed (for flux densities, see Ott et al. 1994 and Mauersberger et al. 1988). All

data were reduced using standard procedures with the CLASS program of the GILDAS software package. For each source, all scans at the same frequency were added to reduce the noise in the final spectrum. All spectra were calibrated to convert the intensity scale from noise diode units to flux density (in Jy), using an updated version of Eq. (1) of Gallimore et al. (2001), which also takes into account gain variations as a function of elevation:

$$\frac{S_\nu}{[\text{Jy}]} = \frac{N}{[\text{counts}]} \times \frac{2.5}{[\text{Jy counts}^{-1}]} \times \begin{cases} [1 - 0.01(30^\circ - \theta^\circ)]^{-1}, & \text{if } \theta^\circ < 30^\circ, \\ 1.0, & \text{if } 30^\circ < \theta^\circ < 60^\circ, \\ [1 - 0.01(\theta^\circ - 60^\circ)]^{-1}, & \text{if } \theta^\circ > 60^\circ, \end{cases}$$

where:

- N is the signal measured by the Effelsberg telescope;
- the third term corrects for the elevation dependent gain of the telescope (θ° : elevation in degrees).

The flux calibration uncertainty is estimated to be of the order of $\pm 10\%$. More observational details are given in Table 1.

2.2. VLA observations of NGC 520, archival data, and imaging

NGC 520 was observed at 22 GHz with the NRAO² Very Large Array (VLA) in the BnA and A configuration on February 14, 2005 and April 17, 2006, respectively. In February 2005 observations were made in Spectral Line Mode, using a single bandwidth of 3.1 MHz, which corresponds to a velocity coverage of $\sim 45\text{ km s}^{-1}$, centered at $V_{\text{LSR}} = 2276\text{ km s}^{-1}$. The use of 256 spectral channels yielded a spacing of 12.2 kHz, corresponding to 0.16 km s^{-1} . In April 2006, NGC 520 was observed both in Spectral and Continuum Mode. For the spectral line observations, we employed the set up used in February 2005, while continuum observations were made using two bands of 50 MHz each, centered at frequencies of 22.4851 and 22.4351 GHz. “Referenced Pointing” observations were made in regular intervals to warrant good antenna pointing. The “Fast Switching” technique was used with a typical duty cycle of 4 min, $\sim 170\text{ s}$ on the target source (NGC 520) and $\sim 70\text{ s}$ on the phase calibrator 0121+043 (0.67 Jy). The flux density scale was established by observing the non-variable source 0137+331 (3C48; 1.13 Jy).

Archival VLA A-array continuum data at 8.5 GHz (project AA296, P.I. Hofner) and 14.9 GHz (project AC156, P.I. Carrol) were also reduced by us. These observations were taken in December 2004 and May 1986, respectively. Absolute calibration was established at 8.5 GHz using 3C 48 (3.15 Jy) and at 14.9 GHz using 3C 286 (3.45 Jy). The compact sources 0125-000 (1.15 Jy) and 0106+013 (3.11 Jy) were measured to calibrate the telescope phases. Furthermore, we have produced two continuum MERLIN³ maps at 1.4 and 5.0 GHz. NGC 520 was observed at 1.4 GHz and 5.0 GHz with the full MERLIN array in December 2000 and November 2004, respectively. For the 1.4 GHz session, the 76-m Lovell telescope took also part in the observations.

All datasets were calibrated in the standard way, except that, since 3C 48 is resolved by the VLA both at 8 and 22 GHz,

² The National Radio Astronomy Observatory is a facility of the National Science Foundation operated under cooperative agreement by Associated Universities, Inc.

³ MERLIN is operated by the University of Manchester as a National facility of the Science and Technology Facilities Council (STFC).

¹ The Effelsberg 100-m telescope is a facility of the MPIfR (Max-Planck-Institut für Radioastronomie) in Bonn.

Table 1. List of galaxies searched for H₂O maser emission.

Source	RA ^a	Dec ^a	V _{sys} ^a	S _{100μm} ^b	V-range ^c	rms	L _{H₂O} ^d	Epoch
	(J2000)	(J2000)	(km s ⁻¹)	(Jy)	(km s ⁻¹)	(mJy)	L _⊙	
NGC 157	00 34 46.7	-08 23 47	1668	37.73	1120, 2220	10	<0.39	21-Jan.-05
NGC 278	00 52 04.3	47 33 02	640	45.16	100, 1180	8	<0.04	21-Jan.-05
NGC 520^e	01 24 35.1	03 47 33	2281	48.40	see Table 3			
NGC 613^e	01 34 18.2	-29 25 07	1475	49.14	see Table 3			
NGC 908	02 23 04.6	-21 14 02	1509	44.43	960, 2060	13	<0.40	21-Jan.-05
NGC 1385	03 37 28.3	-24 30 05	1493	35.62	950, 2040	22	<0.65	19-Jan.-05
UGC 2866	03 50 14.9	70 05 41	1232	49.99	690, 1780	14	<0.29	06-Apr.-04
NGC 1482	03 54 38.9	-20 30 09	1916	46.52	1370, 2470	19	<0.96	10-Apr.-05
NGC 1614	04 33 59.8	-08 34 44	4778	32.38	4210, 5340	14	<3.44	12-Apr.-04
NGC 2339	07 08 20.5	18 46 49	2206	30.24	1660, 2760	9	<0.59	19-Jan.-05
NGC 2566	08 18 45.7	-25 30 03	1637	39.43	1130, 2220	30	<1.12	12-Apr.-04
NGC 3175	10 14 42.1	-28 52 19	1101	31.44	560, 1650	27	<0.44	21-Jan.-05
NGC 3310	10 38 45.9	53 30 12	993	41.76	450, 1540	13	<0.17	06-Apr.-04
MESSIER 95	10 43 57.7	11 42 13	778	35.30	230, 1320	9	<0.07	21-Jan.-05
NGC 3504	11 03 11.2	27 58 21	1534	32.89	990, 2080	8	<0.24	21-Jan.-05
NGC 3593	11 14 37.0	12 49 05	628	35.79	90, 1170	8	<0.04	21-Jan.-05
NGC 3675	11 26 08.6	43 35 09	770	35.20	230, 1310	6	<0.05	21-Jan.-05
NGC 3810	11 40 58.8	11 28 17	993	31.40	450, 1540	9	<0.12	31-Mar.-05
NGC 3893	11 48 38.2	48 42 39	967	35.07	420, 1510	9	<0.11	31-Mar.-05
NGC 4030	12 00 23.6	-01 06 00	1465	46.34	920, 2010	10	<0.28	21-Jan.-05
NGC 4041	12 02 12.2	62 08 14	1234	31.49	690, 1780	14	<0.29	06-Apr.-04
NGC 4157	12 11 04.4	50 29 05	774	43.24	230, 1320	8	<0.07	10-Apr.-05
NGC 4355	12 26 54.6	-00 52 39	2179	33.78	1630, 2730	12	<0.79	19-Jan.-05
NGC 4536	12 34 27.1	02 11 16	1808	44.98	1260, 2360	8	<0.36	31-Mar.-05
NGC 4605	12 39 59.4	61 36 33	143	30.53	-400, 680	13	<0.003	06-Apr.-04
NGC 4654	12 43 56.6	13 07 35	1037	35.26	490, 1580	11	<0.16	10-Apr.-05
UGC 8058	12 56 14.2	56 52 25	12642	30.89	12030, 13250	11	<21.57	06-Apr.-04
NGC 5033	13 13 27.5	36 35 38	875	44.53	330, 1420	11	<0.11	19-Jan.-05
NGC 5078	13 19 50.0	-27 24 36	2168	32.76	1620, 2720	30	<1.93	12-Apr.-04
NGC 5135	13 25 44.0	-29 50 01	4112	30.83	3550, 4670	30	<6.22	11-Apr.-04
NGC 5248	13 37 32.1	08 53 06	1153	43.97	610, 1700	10	<0.19	21-Jan.-05
MESSIER 101	14 03 12.6	54 20 57	241	30.72	-300, 780	17	<0.01	06-Apr.-04
NGC 5676	14 32 46.8	49 27 28	2114	30.61	1560, 2670	9	<0.57	21-Jan.-05
NGC 5713	14 40 11.5	-00 17 21	1899	37.22	1350, 2450	19	<0.92	21-Jan.-05
NGC 5775	14 53 57.6	03 32 40	1681	45.21	1130, 2230	7	<0.26	31-Mar.-05
NGC 5907	15 15 53.7	56 19 44	667	36.01	120, 1210	11	<0.07	07-Apr.-04
NGC 6643	18 19 46.4	74 34 06	1484	31.78	940, 2050	15	<0.44	10-Apr.-05
NGC 6951	20 37 14.1	66 06 20	1424	37.14	880, 1970	12	<0.33	10-Apr.-05
NGC 7469	23 03 15.6	08 52 26	4892	35.22	4330, 5460	8	<2.34	12-Apr.-04
NGC 7541	23 14 43.9	04 32 04	2678	39.93	2120, 3230	11	<1.05	12-Apr.-04
NGC 7771	23 51 24.9	20 06 43	4277	38.78	3710, 4840	11	<2.47	12-Apr.-04

^a Coordinates and velocities are taken from the NASA/IPAC Extragalactic Database (NED). The systemic velocities are given by $V_{\text{sys}} = cz$. The exception is NGC 613 for which the velocity of de Vaucouleurs et al. (1991) has been taken (see also Sect. 3.1).

^b Flux densities at 100 μm are taken from the IRAS Point Source Catalog (Fullmer & Lonsdale 1989).

^c Inspected velocity ranges.

^d Upper limits for maser luminosities are derived from $L_{\text{H}_2\text{O}}/[L_{\odot}] = 0.023 \times S/[\text{Jy}] \times \Delta v/[\text{km s}^{-1}] \times D^2/[\text{Mpc}^2]$, where S is 3 times the rms in Col. 7 and Δv is the channel width, 78 kHz or $\sim 1.04 \text{ km s}^{-1}$.

^e Source name in bold-face: newly detected maser.

Table 2. Interferometric continuum maps of NGC 520.

Band	ν (GHz)	Observation date	Telescope	Weighting	Restoring beam HPBW (")	Position Angle (°)	θ_{max}^a (")	rms (mJy/Ω _b)
L	1.4	10-Dec.-2000	MERLIN	Natural	0.350 × 0.350	0.00	3	0.1
C	5.0	19-Nov.-2004	MERLIN	Tapered 1.3 Mλ	0.187 × 0.123	-51.12	1	0.07
X	8.5	27-Dec.-2004	VLA-A	Uniform	0.223 × 0.215	18.89	7	0.03
U	14.9	10-May.-1986	VLA-A	Natural	0.205 × 0.151	19.81	4	0.1
K	22.1	14-Feb.-2005	VLA-BnA	Natural	0.369 × 0.136	63.21	7	0.5
K	22.5	17-Apr.-2006	VLA-A	Natural	0.112 × 0.084	11.29	1	0.06

^a Largest angular scales that can be imaged.

phase and amplitude correction factors were determined by using CLEAN component models for this source. Each individual dataset was Fourier-transformed using natural weighting (with the exception of the 8.5 GHz map where we used uniform weighting) and then deconvolved using the CLEAN algorithm (Högbom 1974). Table 2 illustrates the details of the continuum maps.

3. Results

Toward two of the 41 observed targets, the Seyfert galaxy NGC 613 and the merging system NGC 520, H₂O maser emission was detected. Figures 1 and 2 show the line profiles, while line parameters are given in Table 3. Below, we summarize the main properties of the two galaxies and their masers.

3.1. NGC 613

NGC 613 is a barred spiral galaxy (de Vaucouleurs et al. 1991), located at a distance of ~ 20 Mpc ($1'' \cong 100$ pc, for $H_0 = 75$ km s⁻¹ Mpc⁻¹). Optical spectroscopy revealed that this galaxy has a composite spectrum, with an HII region and a Seyfert-like contribution simultaneously present (Veron-Cetty & Veron 1986). High resolution radio continuum maps of the inner kpcs of NGC 613 show a linear structure, consisting of three distinct blobs, oriented perpendicular to a ring-like feature of radius ~ 350 pc (Hummel & Jorsater 1992). A large amount of CO has been detected (Elfhag et al. 1996) but high angular resolution images of molecular emission have, so far, not yet been reported.

The H₂O maser profile in NGC 613, shows two distinct components (see Fig. 1). The most luminous one is centered at ~ 1500 km s⁻¹, which is redshifted w.r.t. the systemic velocity of the galaxy, and has a full width to half maximum linewidth of ~ 40 km s⁻¹. A second blueshifted component is seen at ~ 1450 km s⁻¹ and has a linewidth of ~ 20 km s⁻¹. The total isotropic maser luminosity is $\sim 35 L_\odot$. Independently from our observation, the maser was detected by Kondratko et al. (2006) in July 2003. They report a position for the maser coincident with the optical position of the nucleus with an uncertainty of $1''.3$, supporting the association of the maser emission with AGN activity. The comparison of our spectrum, from 2005, with that of Kondratko et al. (2006, their Fig. 1), from 2003, shows that the line profiles are similar. However, in the former, the peak flux density of the component at $V_{\text{LSR}} \sim 1450$ km s⁻¹ appears to be higher. The large linewidth and the presence of not more than two main components, separated by only a few 10 km s⁻¹, may hint at a jet-maser, as proposed by Kondratko et al. (2006). Nevertheless, the H₂O emission is centered on the HI systemic velocity (see Fig. 1) and on the CO centroid velocity (1465 km s⁻¹; Elfhag et al. 1996), which is not common for jet-masers. Characteristically, jet-masers are entirely found at one side of the systemic velocity, either blue- or redshifted (Henkel et al. 2005b).

3.2. NGC 520

NGC 520 is a nearby ($D \sim 30$ Mpc, $1'' \cong 145$ pc, for $H_0 = 75$ km s⁻¹ Mpc⁻¹) merging system, considered to be the result of an encounter between a gas rich and a gas poor disk galaxy (Hibbard & van Gorkom 1996). The remnant nuclei are clearly visible in near infrared *K*-band ($2\mu\text{m}$) images (Stanford & Balcells 1990; Kotilainen et al. 2001). At optical wavelengths, the primary nucleus, which is four times more massive than

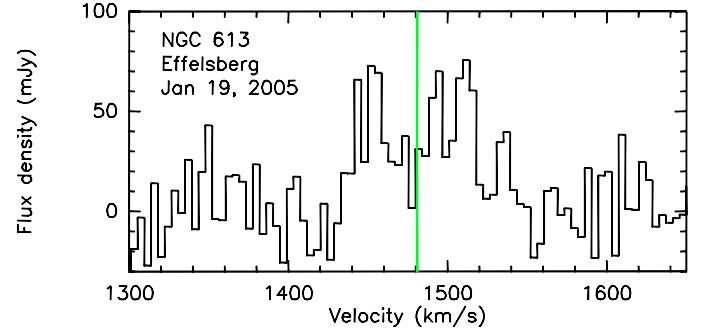


Fig. 1. H₂O megamaser profile observed toward NGC 613 with Effelsberg on January 19, 2005. Channel spacing and pointing position are 4.3 km s⁻¹ and $\alpha_{2000} = 01^{\text{h}}34^{\text{m}}18^{\text{s}}.2$, $\delta_{2000} = -29^{\circ}25'07''$, respectively. The velocity scale is with respect to the local standard of rest (LSR) and uses the optical convention. The vertical line indicates the HI systemic velocity $V_{\text{sys}} = 1481 \pm 5$ km s⁻¹ (NED).

the other (Stanford & Balcells 1990), is hidden behind a pronounced dust lane, while the secondary less massive one is seen $40''$ (6 kpc) to the north-west (Stanford & Balcells 1990; Laine et al. 2003).

The radio continuum emission arising from NGC 520 is confined to a linear east-west structure of $\sim 6''$ (~ 870 pc) in extent, with the peak coinciding with the $2\mu\text{m}$ position of the main nucleus (Condon et al. 1982; Carral et al. 1990; Beswick et al. 2003). The 4.9 GHz unresolved peak source of Condon et al. (1982) is resolved into 3 components in the 14.9 GHz map of Carral et al. (1990). The 14.9 GHz map reveals a total of 5 components, aligned along the linear structure. Beswick et al. (2003) imaged NGC 520 at 1.4 and 1.6 GHz with MERLIN. In their highest resolution map, the linear continuum structure resolves into 10–15 compact components. Five of these coincide with the sources detected by Carral et al. (1990), which Beswick et al. (2003) associated with bright supernova remnants (SNRs) and radio supernovae (RSNe).

The inner 1 kpc surrounding the primary nucleus contains a large concentration of neutral atomic and molecular gas. HI and OH have been detected in absorption, along with an OH maser feature (Beswick et al. 2003). The velocity distribution of both HI and OH trace a kpc-scale ring or disc at a position angle (PA) of 90° rotating about the main nucleus with a velocity gradient of 0.5 km s⁻¹ pc⁻¹. This result is consistent with the CO velocity field (Yun & Hibbard 2001).

Chandra X-ray observations (Read 2005) show no significant diffuse emission from the secondary nucleus, while diffuse emission, consistent with a starburst driven wind, has been discovered outflowing from the primary nucleus, perpendicular to the molecular CO disk (Yun & Hibbard 2001). *Chandra* observations also revealed 15 point sources within the optical boundaries of the galaxy (Read 2005). The third brightest of these, source 12, is an ultraluminous X-ray source (ULX) with $L_X(0.2\text{--}10\text{ keV}) \sim 9 \times 10^{39}$ erg s⁻¹. Since it coincides, within the uncertainty, with the radio peak (Condon et al. 1982), the center of the molecular disk traced by CO (Yun & Hibbard 2001), and the center of the diffuse wind structure, it has been associated with the main nucleus of NGC 520.

3.2.1. The detection and variability of the H₂O maser

On January 21, 2005, we detected a single, narrow H₂O maser line in NGC 520 (see Fig 2). The line parameters are reported

Table 3. Line parameters of newly detected masers.

Source	Adopted distance ^d (Mpc)	Epoch	Tel.	$\int S dV^a$ (mJy km s ⁻¹)	$V_{\text{LSR,opt}}^a$ (km s ⁻¹)	$\Delta V_{1/2}^a$ (km s ⁻¹)	V-range ^b (km s ⁻¹)	Channel Width (km s ⁻¹)	rms (mJy)	$L_{\text{H}_2\text{O}}^c$ (L_{\odot})
NGC 613	20	Jan. 19 2005	Eff	1500 ± 300	1453 ± 2	23 ± 4	930, 2020	4.3	18	14
				2300 ± 300	1502 ± 3	37 ± 6		4.3	18	21
NGC 520	30	Jan. 21 2005	Eff	120 ± 10	2275.28 ± 0.05	1.1 ± 0.6	1730, 2830	1.1	8	2.1
				70 ± 60	2275.42 ± 0.08	0.6 ± 0.2	2010, 2560	0.3	28	1.4
		Feb. 14 2005	VLA	25 ± 2	2275.15 ± 0.03	0.61 ± 0.07	2250, 2300	0.2	4	0.5
		Mar. 31 2005	Eff	2010, 2560	0.3	29	<0.5
		Apr. 10 2005	Eff	1730, 2830	1.1	11	<0.8
		Nov. 14 2005	Eff	2010, 2560	1.1	8	<0.5
Apr. 17 2006	VLA	2250, 2300	0.2	5	<0.1		

^a Integrated flux densities, center velocities, and the full width to half maximum (FWHM) linewidths of the observed features are obtained from Gaussian fits.

^b Inspected velocity ranges.

^c Isotropic luminosities are derived from $L_{\text{H}_2\text{O}}/[L_{\odot}] = 0.023 \times \int S dV/[\text{Jy km s}^{-1}] \times D^2/[\text{Mpc}^2]$.

^d Distances have been estimated using $H_0 = 75 \text{ km s}^{-1} \text{ Mpc}^{-1}$.

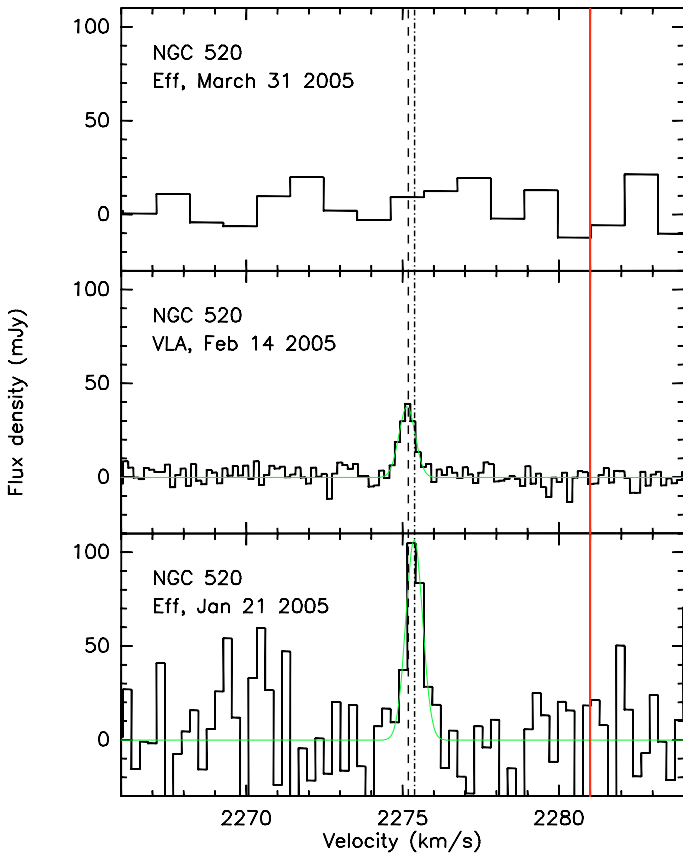


Fig. 2. H₂O kilomaser spectra observed toward NGC 520 between January 21 and March 31, 2005. Channel spacings are 0.3 km s⁻¹ (lower panel), 0.2 km s⁻¹ (middle panel), and 1.1 km s⁻¹ (upper panel). The pointing position is $\alpha_{2000} = 01^{\text{h}}24^{\text{m}}35^{\text{s}}.1$, $\delta_{2000} = +03^{\circ}47'33''$. The solid vertical line indicates the systemic velocity $V_{\text{sys}} = 2281 \text{ km s}^{-1}$ (NED). The dash-dotted and dashed lines represent the peak velocities of the maser in the Effelsberg and VLA spectra, respectively.

in Table 3. The inferred isotropic maser luminosity is $\sim 1 L_{\odot}$. On February 14, the VLA observations confirmed the presence of a single, narrow emission feature. As is evident from Fig. 2 and Table 3, the peak flux density of the line has decreased w.r.t. the earlier Effelsberg spectrum. In addition, a small shift

of $\sim 0.3 \text{ km s}^{-1}$ toward the blue is apparent. A 2-dimensional Gaussian fit (made using AIPS task JMFIT) to an image of the channel maps showing maser emission indicates a spatially unresolved spot at a position $\alpha_{2000} = 01^{\text{h}}24^{\text{m}}34^{\text{s}}.914 \pm 0.001$ and $\delta_{2000} = 03^{\circ}47'29''.79 \pm 0''.01$. The uncertainties of the position are the formal errors determined by JMFIT. These are consistent with the theoretical error given, for each coordinate, by $\sim 0.5\theta_b/\text{SNR}$, where θ_b is the beam (HPBW) size along either RA or Dec and SNR is the signal-to-noise ratio in the map. Having used the “Fast Switching” technique (see Sect. 2.2), the absolute positional accuracy is likely consistent with this value. Nevertheless, for the absolute uncertainty we conservatively take $0''.1$, the canonical error for VLA K-band A-array observations. The position and the velocity of the H₂O maser are incompatible with those of the weak OH masers detected by Baan et al. (1985) and Beswick et al. (2003).

In the Effelsberg observation made on March 31, no emission above the 3σ noise level of $\sim 90 \text{ mJy}$ was found in the 0.3 km s^{-1} wide channels (Fig. 2 shows a smoothed spectrum). The fading of the maser line was confirmed by our most recent spectrum, taken with the VLA on April 17, 2006, with a 3σ detection threshold of 15 mJy for a 0.2 km s^{-1} wide channel. The decrease in flux density of $\sim 70\%$ within 24 days (from January 21 to February 14), implies a size scale $\leq 6.2 \times 10^{16} \text{ cm}$ ($\leq 0.02 \text{ pc}$) or $\leq 0.14 \text{ mas}$ at a distance of 30 Mpc (if variations are intrinsic to the masing cloud(s)). The corresponding brightness temperature is $\geq 10^{10} \text{ K}$.

We produced continuum maps from the VLA line data cubes of February 2005 and April 2006 using the line free channels and find an unresolved spot with a peak flux density of $3\text{--}4 \text{ mJy beam}^{-1}$ at the position of the maser. We compared these maps with the broad band continuum map at 22.1 GHz (see next section). Position and flux density of this source are not compatible with those of the continuum source detected in the broad band map. In order to investigate this ambiguity, we smoothed the line data cubes to a resolution of 0.8 km s^{-1} to increase the signal-to-noise ratio in individual channels. In these maps we see “tentative” weak line emission at a $3\text{--}4\sigma$ level at exactly the same position as the main maser line but at different velocities. We made additional continuum maps excluding these velocity channels and the continuum source is still present at the same position, though with lower flux density. Hence, we think that the spot seen in the line-free maps is likely caused by

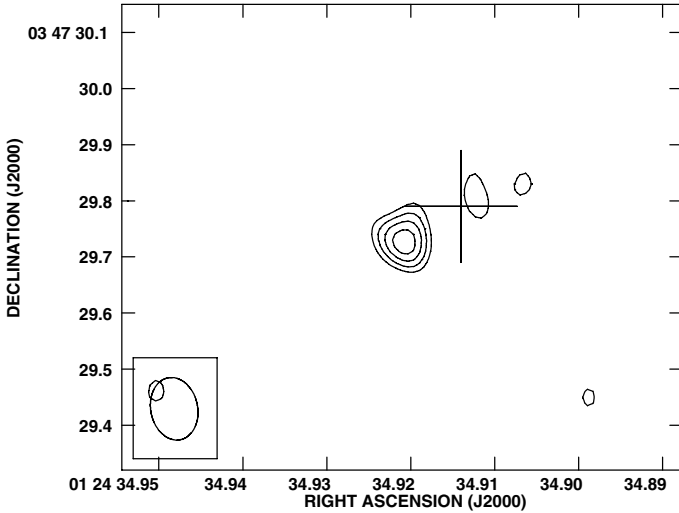


Fig. 3. VLA A-array 22.5 GHz broad band continuum map of NGC 520, from April 17, 2006. Contour levels are $-3, 3, 4, 5, 6 \times 0.06 \text{ mJy beam}^{-1}$. The cross marks the position of the H₂O maser.

the blending of weak maser lines below the detection threshold of the individual channel maps, possibly spread over the entire 45 km s^{-1} bandpass.

3.2.2. The 22 GHz continuum source

In the 22.5 GHz continuum image made from the broad band continuum dataset, we find a single, almost unresolved source (Fig. 3, hereafter labeled “K”), whose position, determined fitting an elliptical Gaussian with JMFIT, is $\alpha_{2000} = 01^{\text{h}}24^{\text{m}}34^{\text{s}}.921 \pm 0.001$ and $\delta_{2000} = 03^{\circ}47'29''.73 \pm 0''.01$. If we assume, as before, that the absolute positional accuracy is $0''.1$, then the uncertainty on the relative positions is $0''.14$. Within this conservatively estimated error the maser and the continuum source coincide. However, as we stated in Sect. 3.2.1, the absolute position error is probably smaller than this value and might even be of order 10 mas. In this case the peaks of the maser and that of source K do not coincide any longer (they are displaced by $0''.12 \pm 0''.014$, or $18 \pm 2 \text{ pc}$). The peak and integrated flux densities of source K are $0.41 \pm 0.07 \text{ mJy beam}^{-1}$ and $0.5 \pm 0.1 \text{ mJy}$, respectively. The undeconvolved extent is $110 \pm 20 \times 100 \pm 20 \text{ mas}$ with position angle (PA) $\sim +30^\circ$, matching the size and PA of the beam. The brightness temperature of the source is $\geq 40 \text{ K}$.

3.2.3. Nuclear continuum sources

Figure 4 shows the MERLIN and VLA images of the inner $6'' \times 2''.5$ region surrounding the main nucleus of NGC 520 at the frequencies of 1.4, 5.0, 8.5, and 14.9 GHz (details of these maps are given in Table 2). Consistent with previous studies (e.g. Carral et al. 1990; Beswick et al. 2003), a linear east-west structure is visible at all frequencies. This structure is resolved into several compact components, the number of which depends on the resolution and sensitivity of the maps. In our maps it is possible to identify a total of 7 compact sources, labeled with the letters A to G. The four sources A, B, C, and F, are resolved into sub-components in the MERLIN C-band and VLA U-band maps, because of their higher resolution. Coordinates, peak and integrated flux densities are displayed in Table 4 for

the MERLIN maps and in Table 5 for the VLA data. From a comparison with previously published radio continuum maps, we can associate our five sources A–E with those labeled C1–C5 of Carral et al. (1990) and 4–8 of Beswick et al. (2003). It is, however, not possible to associate the other two sources, F and G, with any of the sources reported by Carral et al. (1990) or Beswick et al. (2003).

For all maps, with the exception of the MERLIN L-Band one, the parameters (peak coordinates and peak and integrated flux densities; Tables 4 and 5) were derived fitting a 2-dimensional Gaussian (AIPS task: JMFIT). In the L-Band map, positions were measured using the AIPS task IMSTAT, which reads a portion of an image and provides the location and value of the maximum brightness in that portion. Integrated flux densities were obtained using the task BLSUM, which sums the pixels’ flux densities over blotch polygonal regions. The blotch areas over which to integrate were determined according to the average dimensions of the source (as derived from the other maps) in order to avoid confusion with the extended background present in the L-Band map. The flux density uncertainties reported in the two tables (4 and 5) are provided directly by the tasks used and range between a few percent up to 20 percent of the values measured.

At 6 cm, the longest baseline, B_{max} , of MERLIN (215 km) provides a resolution of $\sim 0.05''$ that is a factor of 6 better than that of the VLA in its most extended configuration. Therefore, MERLIN maps can resolve a source seen by the VLA as one in two or more components (e.g. our sources A and C). In addition, since the shortest baseline, B_{min} , of MERLIN is 9 km, while that of the VLA A-array is 0.68 km, the two instruments have quite a different response to extended structure (see also Table 2): at 6 cm, the MERLIN interferometer is “blind” to emission more extended than $1''$ while the VLA can map emission on a $10''$ – $15''$ scale. This latter problem, which is obvious when comparing our 5.0 GHz MERLIN map with the others (Fig. 3.2.2), will affect the computation of the peak flux densities and integrated fluxes. The background of the MERLIN L-Band and the VLA maps is resolved-out in the C-Band where, rather, a bowl-like depression is created, which reduces the values of the peak flux densities (see e.g., Wills et al. 1998). Furthermore, some extended emission in the larger of the compact sources may also be missed in the calculation of the integrated fluxes. For this reason, we have decided not to use the 5.0 GHz MERLIN data in our computation of the spectral indices. In addition, due to the lower resolution of the L-Band MERLIN images some sources are blended, and hence, we have also not used this image for the spectral index estimates. Nevertheless, it is useful to show the MERLIN maps in order to compare the global morphology of the radio emission from NGC 520 at different frequencies and to potentially spot new sources (e.g. new radio supernovae) that might serendipitously appear in galaxies with high star formation rates.

Spectral indices were then computed from the VLA maps at 8.5 and 14.9 GHz following the convention $S \propto \nu^\alpha$. The resolution of the two maps is almost identical, and therefore, a convolution to the same beam was not necessary. The last two columns of Table 5 show the computed spectral indices using both peaks and integrated fluxes. The errors on the spectral index α were derived using the standard equation for error propagation,

$$\Delta\alpha = \pm \frac{0.434}{\lg \nu_2 - \lg \nu_1} \sqrt{\left(\frac{\Delta S_{\nu_1}}{S_{\nu_1}}\right)^2 + \left(\frac{\Delta S_{\nu_2}}{S_{\nu_2}}\right)^2},$$

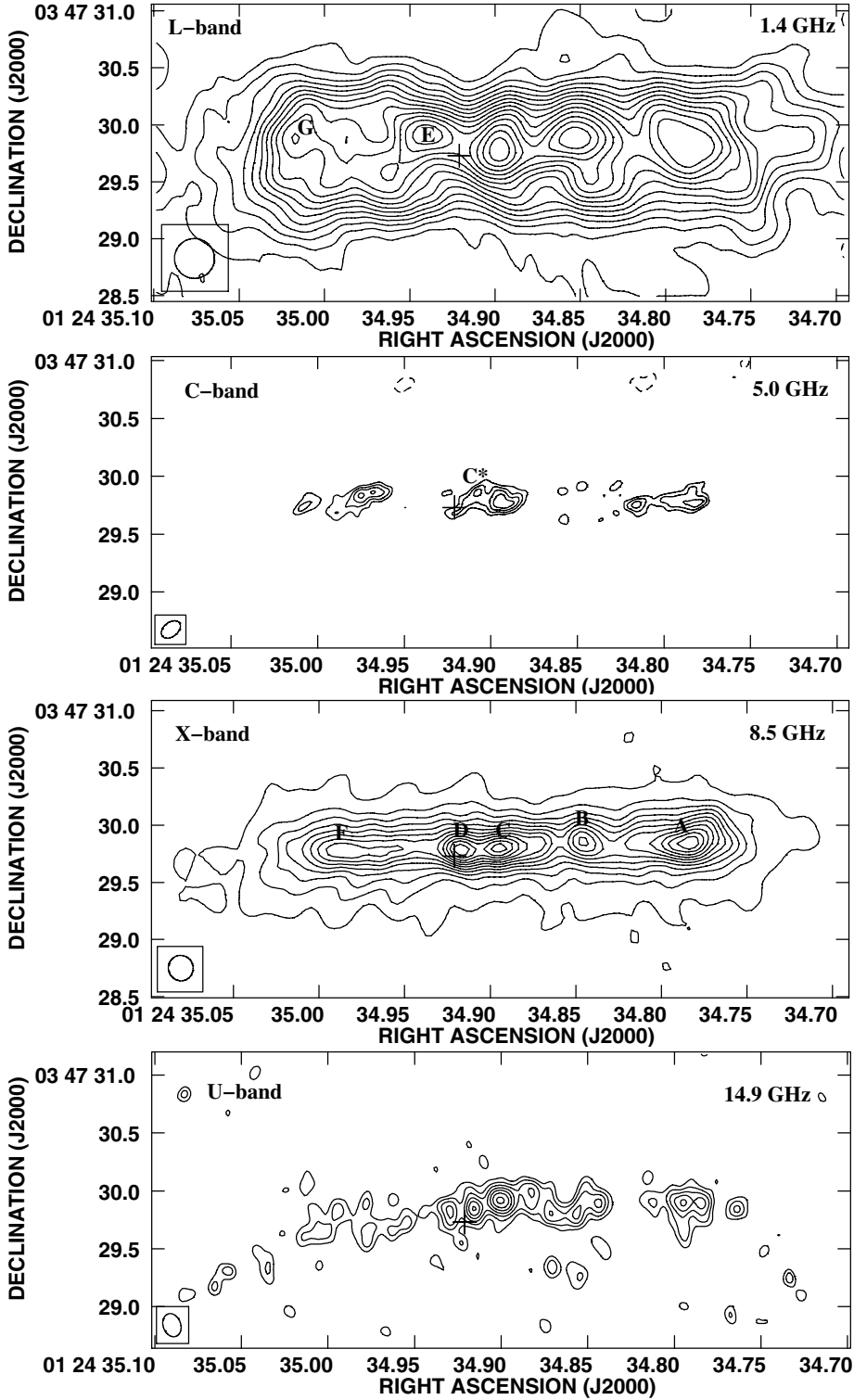


Fig. 4. Radio continuum contour maps of the nuclear region of NGC 520 with labels indicating the compact sources A–G. From top to bottom: L-band, MERLIN, contour levels are $-3, 3, 6, 9, 12, 15, 18, 21, 24, 27, 30, 33, 36, 39, 42, 45, 48 \times 0.1 \text{ mJy beam}^{-1}$; C-band, MERLIN, contour levels are $-3, 3, 4, 5, 6 \times 0.1 \text{ mJy beam}^{-1}$; X-band, VLA, contour levels are $-1, 1, 2, 3, 4, 5, 6, 7, 8, 9, 10, 11, 12, 13, 14, 15, 16 \times 0.1 \text{ mJy beam}^{-1}$; U-band, VLA, contour levels are $-3, 3, 4, 5, 6, 7, 8, 9 \times 0.1 \text{ mJy beam}^{-1}$. The cross marks the position of continuum source K detected at 22 GHz (Fig. 3).

where ν , S_ν , and ΔS_ν are the frequency, flux density, and error of the flux density, respectively. The subscripts “1” and “2” refer to frequencies 8.5 and 14.9 GHz, correspondingly.

4. Discussion

4.1. The FIR sample

The FIR sample of intermediate bright galaxies ($30 < S_{100\mu\text{m}} < 50 \text{ Jy}$) comprises 40 spirals and a galaxy pair (NGC 520).

Among them, 14 are starburst galaxies and only 10 are classified as Seyferts. As for the FIR sample of brighter galaxies ($S_{100\mu\text{m}} > 50 \text{ Jy}$; see Henkel et al. 2005b), there are very few galaxies with FIR luminosities greater than $10^{11} L_\odot$ in our sample. There are only four Luminous Infrared Galaxies (LIRGs, with $L_{\text{FIR}} > 10^{11} L_\odot$), NGC 1614, NGC 5135, NGC 7469, and NGC 7771 and one Ultraluminous Infrared Galaxy (ULIRG, $L_{\text{FIR}} > 10^{12} L_\odot$), UGC 8058.

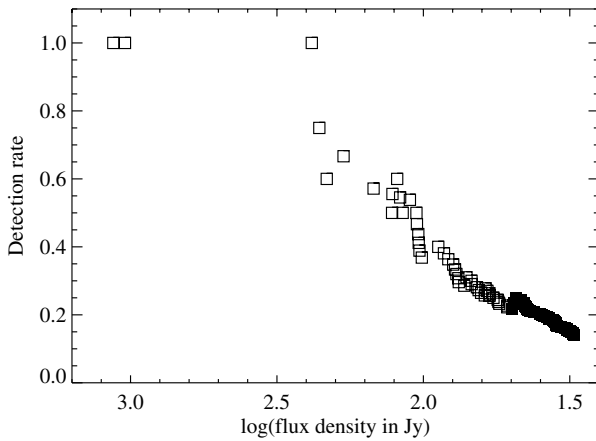
Adding the result of our “intermediate-range” sample, i.e. two new maser detections (NGC 613 and NGC 520) out of 41

Table 4. Properties of the nuclear continuum sources in NGC 520 observed with MERLIN at 1.4 and 5 GHz.

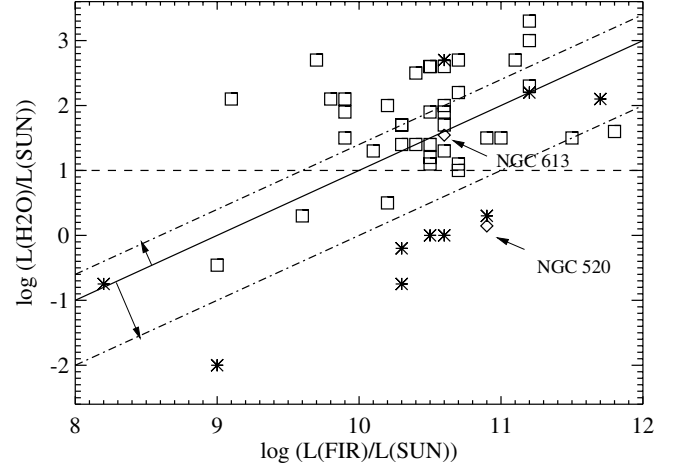
Label	α	δ	$\nu = 1.4$ GHz		$\nu = 5.0$ GHz	
	(J2000) 01 ^h 24 ^m	(J2000) 03°47'	Peak flux (mJy/ Ω_b)	Total flux (mJy)	Peak flux (mJy/ Ω_b)	Total flux (mJy)
A	34°78	29''8	3.5 ± 0.1	4.7 ± 0.3	0.56 ± 0.08	1.0 ± 0.2
	34°82	29''8			0.55 ± 0.07	0.55 ± 0.07
B	34°85	29''9	4.5 ± 0.1	4.5 ± 0.1	0.38 ± 0.07	0.38 ± 0.07
	34°86	29''9			0.35 ± 0.07	0.35 ± 0.07
C	34°90	29''8	4.8 ± 0.1	5.4 ± 0.4	0.69 ± 0.08	2.3 ± 0.3
C*	34°91	29''9			0.54 ± 0.07	0.54 ± 0.07
D	34°92	29''8	<0.3	...	<0.2	...
E	34°93	29''8	4.2 ± 0.1	4.2 ± 0.1	<0.2	...
F	34°97	29''9	3.4 ± 0.1	3.4 ± 0.1	0.62 ± 0.07	0.62 ± 0.07
	34°98	29''8			0.62 ± 0.07	0.62 ± 0.07
G	35°01	29''7	3.3 ± 0.1	3.3 ± 0.1	0.44 ± 0.07	0.44 ± 0.07

Table 5. Properties of the nuclear continuum sources in NGC 520 observed with the VLA at 8 and 15 GHz.

Label	α	δ	$\nu = 8.5$ GHz		$\nu = 14.9$ GHz		$\alpha_{15,p}^8$	$\alpha_{15,i}^8$
	(J2000) 01 ^h 24 ^m	(J2000) 03°47'	Peak flux (mJy/ Ω_b)	Total flux (mJy)	Peak flux (mJy/ Ω_b)	Total flux (mJy)	Spectral index (from peaks)	Spectral index (from integrated fluxes)
A	34°78	29''8	1.18 ± 0.03	5.7 ± 0.2	0.7 ± 0.1	2.2 ± 0.1	-0.8 ± 0.2	-1.5 ± 0.4
B	34°85	29''9	0.97 ± 0.03	0.97 ± 0.03	0.6 ± 0.1	0.6 ± 0.1	-0.8 ± 0.3	-0.8 ± 0.3
	34°86	29''9			0.6 ± 0.1	0.6 ± 0.1		
C	34°90	29''8	1.27 ± 0.03	4.2 ± 0.1	0.9 ± 0.1	2.5 ± 0.4	-0.5 ± 0.2	-0.8 ± 0.3
D	34°92	29''8	1.29 ± 0.03	1.29 ± 0.1	0.8 ± 0.1	0.8 ± 0.1	-0.8 ± 0.3	-0.8 ± 0.3
E	34°93	29''8	<0.1	...	0.6 ± 0.1	0.6 ± 0.1		
F	34°97	29''9	0.90 ± 0.03	5.5 ± 0.2	<0.3	...		
G	35°01	29''7	<0.1	...	<0.3	...		

**Fig. 5.** H₂O maser cumulative detection rate above a certain 100 μ m IRAS Point Source Catalog flux density for the parent galaxy. The figure is a modified version of Fig. 13 of Henkel et al. (2005b). Filled squares represent our values derived using the “intermediate-luminosity” sample.

galaxies searched, to that of Henkel et al. (2005b), the cumulative detection rate above a 100 μ m IRAS Point Source Catalog flux of 30 and 40 Jy for the parent galaxy becomes 14% and 20%, respectively (Fig. 5). When considering the detection rate related to the specific FIR flux density interval (30–50 Jy) of our sample, we obtain 2/41 or 5%. The two detected galaxies, NGC 613 and NGC 520, are the second and third FIR-brightest galaxies of the sample. The FIR-brightest galaxy of the sample,

**Fig. 6.** H₂O vs. FIR luminosity plot including our two new maser detections, NGC 613 and NGC 520, and the separation between the kilomaser and megamaser regimes (dashed line). Open squares represent most of the 22 GHz extragalactic H₂O masers detected so far (Henkel et al. 2005b). The asterisks indicate the remaining 10 maser sources belonging to the FIR subsample with $S_{100\mu\text{m}} > 50$ Jy (see Henkel et al. 2005b). The solid line marks the correlation for Galactic star-forming regions (Jaffe et al. 1981). The upper and lower dot-dashed diagonal lines show the FIR/H₂O luminosity relations for the mega- and kilomasers, respectively, with the slope being fixed to that of the Jaffe et al. (1981) correlation.

UGC 2866, thus might also be detectable if frequent monitoring is performed (nota bene the high degree of variability we see in NGC 520!).

Henkel et al. (2005b) found a rough proportionality between L_{FIR} and $L_{\text{H}_2\text{O}}$ for extragalactic water masers. When plotting the value for NGC 613 into this diagram (Fig. 6), it follows the relationship representing the $L_{\text{FIR}}/L_{\text{H}_2\text{O}}$ correlation for Galactic masers found by Jaffe et al. (1981). The point representing NGC 520 is, however, located well below the line of the correlation. This system has either an excess in L_{FIR} w.r.t. $L_{\text{H}_2\text{O}}$ or its maser luminosity is particularly low. Most likely, the bulk of the 22 GHz H₂O emission remains undetected because of limitations in sensitivity (see the Sect. 3.2.1). When taking a closer look at the $L_{\text{FIR}}/L_{\text{H}_2\text{O}}$ plot and considering megamaser and kilomaser sources separately (above and below the dashed $L_{\text{H}_2\text{O}} = 10 L_{\odot}$ dividing line), the two groups seem to follow independent correlations. While H₂O kilomasers are “subluminous” for a given L_{FIR} w.r.t. Galactic star-forming regions (Jaffe et al. 1981), the megamasers appear to be slightly “superluminous”. The two samples diverge by ~ 1.5 orders of magnitude in maser luminosity for a given FIR luminosity, emphasizing their different origin.

4.2. NGC 520

4.2.1. Where is the nucleus?

Our measurements place the kilomaser in NGC 520 in the innermost nuclear region of the galaxy. In order to associate the maser emission with either enhanced star formation or with nuclear activity, we have first to locate and identify the galaxy’s true nucleus and check whether it exhibits (low-luminosity) AGN activity. So far, no clear evidence for the presence of an AGN in NGC 520 has been reported. It is impossible to determine the spectral type of the main nucleus on the basis of its optical spectrum because of a lack of diagnostic emission lines (Veilleux et al. 1995). This is likely due to the large extinction suffered by the main nucleus (see Sect. 3.2). However, an indication of absent (or weak) nuclear activity is the presence of PAH features in the mid-infrared spectrum (Brandl et al. 2006), which should be diluted by the strong infrared continuum of an AGN (Krolik 2001). No Fe-K line seems to be present in the X-ray spectrum but an ULX source (source 12, see Sect. 3.2) with a “power law spectrum” ($N_{\text{H}} = 2.3 \times 10^{22} \text{ cm}^{-2}$) is detected close to the main nucleus (Read 2005). Figure 7 shows a plot in which the positions for the main centers of activity are marked. The X-ray source 12 lies closest to radio source C (see Sect. 3.2.3) and, according to Read (2005), is “undoubtedly associated with the primary nucleus of NGC 520”. However, due to the uncertainty of Chandra’s absolute astrometry the error circle ($\approx 0''.7$) also encompasses sources D and K. Which is, then, the true nucleus of the galaxy?

Source K is close to sources C (further resolved into a double source in the MERLIN C-Band image) and D. Assuming the conservative accuracy of $0''.1$ ($\equiv 15 \text{ pc}$ at a distance of 30 Mpc; see Fig. 3.2.2) for the absolute positions in all the VLA maps, source K cannot be associated with source C, but an association with D is possible (the angular distance is $\sim 0''.07$; see Fig. 7). The slightly-resolved source C has a spectral index between 8.5 and 14.9 GHz, α_{15}^8 , of -0.5 ± 0.2 (from the peak flux densities) and of -0.8 ± 0.3 (from the integrated fluxes; see Table 5). If the slope of the spectrum still holds at higher frequencies, it is possible to derive the expected integrated intensities for source C at 22.5 GHz, $1.8 \pm 0.4 \text{ mJy}$. In order to make the integrated fluxes for source C and K consistent, a spectral index α_{22}^{15} of ≈ -4 would be necessary, which is impossible to justify with standard physical models. For source D, the spectral index is $\alpha_{15}^8 = -0.8 \pm 0.3$, providing an expected value for the 22.5 GHz integrated

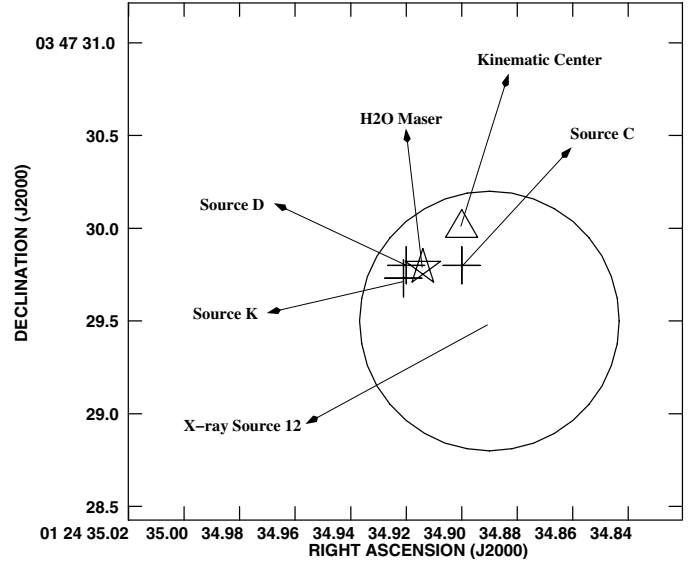


Fig. 7. Positions of the main centers of activity in the nuclear region of NGC 520. The plus signs mark the radio continuum sources C, D, and K detected in our VLA maps, while the five-pointed star indicates the position of the H₂O maser (this paper). The triangle identifies the kinematic center derived from CO and HI studies (Yun & Hibbard 2001). The circle indicates the luminous X-ray source (labeled 12) detected by Read (2005) using Chandra. The sizes of the marks denote absolute positional accuracies.

intensity of $0.6 \pm 0.1 \text{ mJy}$. This value agrees within the uncertainties with that of source K ($0.5 \pm 0.1 \text{ mJy}$; see Sect. 3.2.2), making the association between the two sources, D and K, the most convincing option. Given this interpretation, it remains quite surprising that no other source, and especially source C, is detected at 22.5 GHz. The non-detection of source C must be a consequence of its angular extent, confirmed also by the MERLIN C-Band map. The other sources are likely too weak to be detected in our highest frequency map due to their non-thermal nature.

What, then, is the nature of source K (or D)? Its size is smaller than $0''.1$ ($\equiv 15 \text{ pc}$) and its spectrum is characterized by a steep radio spectral index, which is consistent with optically thin synchrotron emission from a RSN or a young *SNR*, similar to the situation found in other starburst galaxies like M 82 (e.g., McDonald et al. 2002) and NGC 2146 (Tarchi et al. 2000). The luminosity of source K (or D) at 5 GHz (extrapolating the flux density from the 8.5 GHz value using a spectral index of -0.8 ; Table 5) is $\approx 2 \times 10^{20} \text{ W Hz}^{-1}$, which is greater than the luminosity of the strongest non-thermal compact source found in M 82, but comparable with the luminosities of SNRs found in other merger systems, like Arp 299 and Arp 220 (Fig. 8). However, when plotting the surface brightness of source K ($\sim 8 \times 10^{-17} \text{ W Hz}^{-1} \text{ m}^{-2} \text{ sr}^{-1}$) as a function of its diameter (15 pc) in the Σ -D diagram for the SNRs in M 82, NGC 2146, Arp 299 and Arp 220 (Fig. 9), the value is incompatible with those obtained for the other sources (with the exception of the SNRs in Arp 220). Being spatially unresolved, the derived source size is an upper limit, and hence, the position of source K might move toward the upper-left corner of the plot, where the strongest sources in M 82, NGC 2146, and Arp 299 lie. Nevertheless, the anomalous position of source K in the Σ -D plot might also suggest that it is a low luminosity AGN (LLAGN). Indeed, radio observations of Seyfert and LINER galaxies show that LLAGN may have steep radio spectral indices (Morganti et al. 1999; Krips et al. 2007) and luminosities comparable to

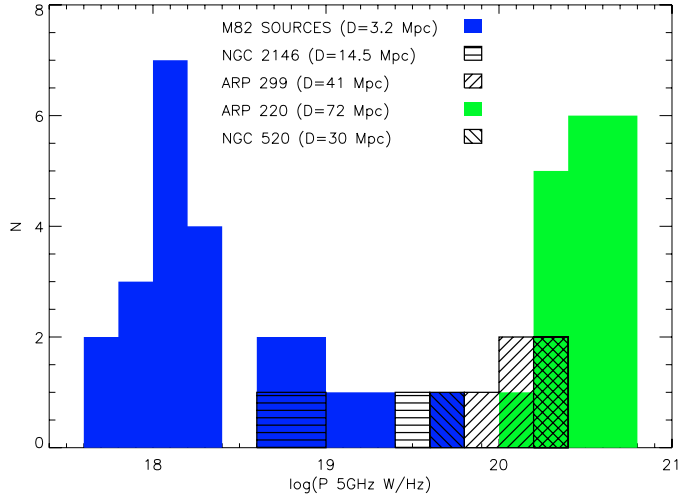


Fig. 8. 5 GHz luminosity distribution of the non thermal sources C, C*, and D (or K) (for this source the flux density has been extrapolated from the 8 GHz VLA map using the spectral index reported in Table 5) in NGC 520 (this paper), compared with the SNRs in M82 (Muxlow et al. 1994), NGC 2146 (Tarchi 2001, Ph.D. Thesis), Arp 299 (Neff et al. 2004), and Arp 220 (Parra et al. 2007).

that of source K (Morganti et al. 1999). In summary, the parameters derived for source K (or D), viz. spectral indices, luminosities and diameter, are consistent both with those of SNRs and LLAGNs. Multi-epoch and/or multi-frequency VLBI observations would be necessary to select between the two options.

Source C has also a steep spectral index, a large luminosity ($2.3 \times 10^{20} \text{ W Hz}^{-1}$ at 5.0 GHz) and a position in the Σ -D diagram which does not match those of the other sources (Fig. 9). However, one of the key points that determine its position in the aforementioned diagram is its size, which we estimate to be of order $0''.3$ (≈ 40 pc). This size is too large to justify a possible LLAGN nature, and hence, we think that source C is a particularly active star-forming region composed of a collection of small and young SNRs/RSNe that we do not fully resolve. This is also suggested by our C-Band MERLIN map that shows the presence of at least one further emission spot (C*, Table 4) close to what we identify as source C. This spot has a size $\leq 0''.2$ (≈ 30 pc), a 5 GHz luminosity of $\approx 5.5 \times 10^{19} \text{ W Hz}^{-1}$, and a surface brightness $\geq 5.7 \times 10^{-18} \text{ W m}^2 \text{ Hz}^{-1} \text{ sr}^{-1}$. These properties are more consistent with those of SNRs (see Figs. 8 and 9), supporting our interpretation. Also, the kinematic center, although close-by, is not coincident with source C favoring a different view from that suggested by Read (2005). Given this, it still remains unclear where the nucleus of the galaxy is located, but if a LLAGN exists in NGC 520, it is likely associated with source D.

4.2.2. The H₂O maser in NGC 520: star formation or nuclear activity?

The association of the maser with source K (or D) is based on the assumption that the uncertainty in the absolute positions is $0''.1$ in our 22 GHz VLA maps (see Sect. 3.2.2). If a less conservative value is assumed, line and continuum do not coincide anymore. Therefore, the maser might not be directly associated with any of the continuum sources. Nevertheless, the small projected distance between the maser spot and source K suggests that the H₂O emission is in some way related to this source. The characteristics of the maser line, i.e. narrowness and strong time

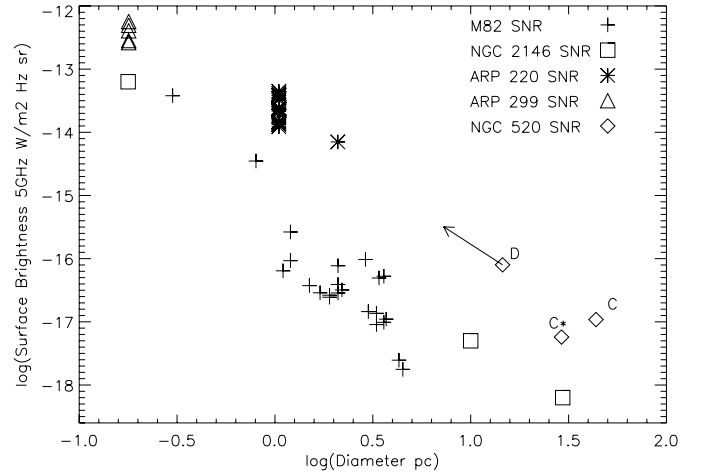


Fig. 9. Σ -D relation for SNRs in M82 (crosses; Muxlow et al. 1994), NGC 2146 (squares; Tarchi 2001, Ph.D. Thesis and Surcis, 2004, Ph.D. Thesis), Arp 299 (triangles; Neff et al. 2004), Arp 220 (asterisks; Parra et al. 2007), and the sources C, C*, and D (or K) (diamonds) in NGC 520 (this paper). The arrow shows the direction into which source D would be moved, if its size would be <15 pc.

variability (70% decrease of the flux density within 24 days) are more consistent with star formation than with nuclear activity. Narrow flaring components are common in water maser emission from Galactic star-forming regions, although only the outbursts in W49N reached a luminosity comparable to that of NGC 520 (Liljeström & Gwinn 2000; Honma et al. 2004). Narrow extragalactic H₂O maser lines have been detected, so far, also in IC 10 (Henkel et al. 1986) and IC 342 (Tarchi et al. 2002b). Both these kilomasers are definitely associated with star-forming regions and have shown a great deal of time variability. The flare of the -324 km s^{-1} component in IC 10 reached $\sim 4 L_{\odot}$ or 120 Jy (Baan & Haschick 1994) only to decay to sub-Jy levels more recently (Brunthaler et al. 2007). Even more similar to the H₂O maser in NGC 520 is the maser in IC 342 reported by Tarchi et al. (2002b). Although less luminous ($L_{\text{H}_2\text{O}} = 10^{-2} L_{\odot}$), the feature was narrow ($\sim 0.6 \text{ km s}^{-1}$) and varied by a factor of 3 within 5 days (Tarchi et al. 2002b). Moreover, for the maser in IC 342, a velocity shift by 1 km s^{-1} was observed within two weeks. The shift and the rapid decay in flux was explained in terms of a chance alignment of two dense molecular clouds.

A similar scenario is also compatible with the maser in NGC 520. When comparing our highest velocity resolution spectra taken with Effelsberg on January 2005 with that taken with the VLA a month later, a small velocity shift seems present. A Gaussian fit to the maser lines indicates velocities of 2275.42 ± 0.08 and 2275.15 ± 0.03 for the Effelsberg and the VLA, respectively (Fig. 2). The velocity shift is $0.27 \pm 0.09 \text{ km s}^{-1}$, i.e. it may be significant. We may assume that both the flare and the shift (if real) have a kinematic origin, following the scenario proposed by Tarchi et al. (2002b). Assuming a negligible distance between the two clouds w.r.t. the distance of the galaxy and a relative velocity in the plane of the sky of $\sim 100 \text{ km s}^{-1}$, this implies a cloud velocity gradient of up to $0.23 \text{ km s}^{-1}/\text{AU}$ during our monitoring time (24 days). Alternatively, the maser feature may be explained by a change in the relative intensities of the three main hyperfine components (see e.g., Fiebig & Guesten 1989) or by a variation in the relative intensity of different emitting regions leading to a swapping-over of velocity peaks (see e.g., Wu et al. 1999). For maser flux density variations (distinct from flares)

due to refractive interstellar scintillations, time scales range from about one month (slightly longer than the variability time scale in NGC 520) to few months (Simonetti et al. 1993). Diffractive scintillation may instead allow for extremely rapid variations (as short as a few minutes) but has been reported, so far, in only two cases, viz. the Circinus Galaxy (Greenhill et al. 1997) and NGC 3079 (Vlemmings et al. 2007).

Although the attributes of the maser (low luminosity, narrowness, and strong variability) hints at an association with star formation, we cannot rule out the possibility that we have found a weak nuclear kilomaser, as the ones in M 51 and (possibly) NGC 4051, perhaps related to a nuclear jet that is too weak to be seen in our radio maps. However, no high-velocity lines blue- or redshifted with respect to the systemic velocity are detected in NGC 520 and this does not support the possibility that the maser is tracing an accretion disk. In addition, the linewidth of the maser feature in NGC 520 ($\sim 0.6 \text{ km s}^{-1}$) is very small compared to the typical linewidth of H₂O masers associated with nuclear jets (e.g., Mrk 348, Peck et al. 2003; M 51, Hagiwara 2007). Most of all, no convincing evidence of an AGN of whatever intensity comes from any study performed so far, making the latter alternative unlikely. However, also a few megamaser galaxies, seen edge on and thus being extremely obscured (like NGC 520), do not show the presence of an AGN (Greenhill et al. 2003b; Braatz et al. 2004).

5. Conclusions

We have observed a sample of 41 galaxies with 100 μm IRAS point source flux density between 30 and 50 Jy and declination $> -30^\circ$, to search for 22 GHz H₂O maser emission. The survey yielded two detections, a megamaser with isotropic luminosity, $L_{\text{H}_2\text{O}}$, of $\approx 35 L_\odot$ in the Seyfert/HII galaxy NGC 613 (see also Kondratko et al. 2006) and a kilomaser with $L_{\text{H}_2\text{O}} \approx 1 L_\odot$ in the merger system NGC 520. Our results confirm the correlation between maser detection rate and FIR flux density discovered by Henkel et al. (2005b) for the sample of galaxies with $S_{100\mu\text{m}} > 50 \text{ Jy}$. When we compare the isotropic luminosity of extragalactic masers with the FIR luminosity of their parent galaxy, we find that kilomasers are “subluminous” while megamasers are “superluminous” for a given L_{FIR} w.r.t Galactic H₂O masers in massive star-forming regions. We agree with Kondratko et al. (2006) that the maser in NGC 613 is possibly associated with the nuclear jet, although the fact that the H₂O emission is centered on the systemic velocity is unusual for a jet-maser and may hint at a different origin.

The kilomaser in NGC 520 has been observed at subarc-second resolution with the VLA. We have found that the H₂O emission arises from the inner hundred parsecs surrounding the dominant nuclear region of the merger system. Assuming an absolute position accuracy of $0''.1$ ($\approx 15 \text{ pc}$), the maser coincides with a continuum source (source K, or D). A spectral index analysis, as well as its general properties, i.e., its size and luminosity, indicate a young *SNR* or a LLAGN. The small linewidth ($\sim 0.6 \text{ km s}^{-1}$) and the time variability (70% decrease of the flux density within 24 days) of the maser feature suggest a size limit of $\leq 0.02 \text{ pc}$ and a brightness temperature greater than 10^{10} K , if the fluctuation is not caused by a variable background continuum source. The H₂O maser emission is most likely associated with star formation, like the majority of kilomasers. Narrowness and variability of the maser feature resemble those of two other kilomasers observed in IC 10 and IC 342 that are associated with star formation. We consider an association with an AGN a less viable option based on the lack of clear traces of AGN activity.

Acknowledgements. This work has benefited from research funding from the European Community’s sixth Framework Programme under RadioNet R113CT 2003 5058187. We wish to thank R.J. Beswick for kindly making available MERLIN 1.4 and 5.0 GHz data on NGC 520 and an anonymous referee for critically reading the manuscript. P.C. and A.T. wish to thank the operators at the 100-m telescope for their hospitality during the observing runs. This research has made use of the NASA/IPAC Extragalactic Database (NED), which is operated by the Jet Propulsion Laboratory, Caltech, under contract with NASA. This research has also made use of the NASA’s Astrophysics Data System Abstract Service (ADS).

References

- Baan, W. A., & Haschick, A. 1994, *ApJ*, 424, L33
 Baan, W. A., Haschick, A. D., Buckley, D., & Schmelz, J. T. 1985, *ApJ*, 293, 394
 Barvainis, R., & Antonucci, R. 2005, *ApJ*, 628, L89
 Baudry, A., & Brouillet, N. 1996, *A&A*, 316, 188
 Beswick, R. J., Pedlar, A., Clemens, M. S., & Alexander, P. 2003, *MNRAS*, 346, 424
 Braatz, J. A., Wilson, A. S., & Henkel, C. 1996, *ApJS*, 106, 51
 Braatz, J. A., Henkel, C., Greenhill, L. J., Moran, J. M., & Wilson, A. S. 2004, *ApJ*, 617, L29
 Brandl, B. R., Bernard-Salas, J., Spoon, H. W. W., et al. 2006, *ApJ*, 653, 1129
 Brunthaler, A., Reid, M. J., Falcke, H., Henkel, C., & Menten, K. M. 2007, *A&A*, 462, 101
 Carral, P., Turner, J. L., & Ho, P. T. P. 1990, *ApJ*, 362, 434
 Churchwell, E., Witzel, A., Huchtmeier, W., et al. 1977, *A&A*, 54, 969
 Claussen, M. J., & Lo, K.-Y. 1986, *ApJ*, 308, 592
 Claussen, M. J., Diamond, P. J., Braatz, J. A., Wilson, A. S., & Henkel, C. 1998, *ApJ*, 500, L129
 Condon, J. J., Condon, M. A., Gisler, G., & Puschell, J. J. 1982, *ApJ*, 252, 102
 de Vaucouleurs, G., de Vaucouleurs, A., Corwin, Jr., H. G., et al. 1991, *Third Reference Catalogue of Bright Galaxies* (Berlin, Heidelberg, New York: Springer-Verlag), 1, 2069
 Elfhag, T., Booth, R. S., Hoeglund, B., Johansson, L. E. B., & Sandqvist, A. 1996, *A&AS*, 115, 439
 Fiebig, D., & Guesten, R. 1989, *A&A*, 214, 333
 Fullmer, L., & Lonsdale, C. J. 1989, *JPL D-1932*, Version 2, part No. 3
 Gallimore, J. F., Henkel, C., Baum, S. A., et al. 2001, *ApJ*, 556, 694
 Greenhill, L. J., Jiang, D. R., Moran, J. M., et al. 1995, *ApJ*, 440, 619
 Greenhill, L. J., Ellingsen, S. P., Norris, R. P., et al. 1997, *ApJ*, 474, L103
 Greenhill, L. J., Booth, R. S., Ellingsen, S. P., et al. 2003a, *ApJ*, 590, 162
 Greenhill, L. J., Kondratko, P. T., Lovell, J. E. J., et al. 2003b, *ApJ*, 582, L11
 Hagiwara, Y. 2007, *AJ*, 133, 1176
 Hagiwara, Y., Henkel, C., Menten, K. M., & Nakai, N. 2001, *ApJ*, 560, L37
 Hagiwara, Y., Diamond, P. J., Miyoshi, M., Rovilos, E., & Baan, W. 2003, *MNRAS*, 344, L53
 Henkel, C., Guesten, R., Downes, D., et al. 1984, *A&A*, 141, L1
 Henkel, C., Wouterloot, J. G. A., & Bally, J. 1986, *A&A*, 155, 193
 Henkel, C., Braatz, J. A., Greenhill, L. J., & Wilson, A. S. 2002, *A&A*, 394, L23
 Henkel, C., Tarchi, A., Menten, K. M., & Peck, A. B. 2004, *A&A*, 414, L17
 Henkel, C., Braatz, J. A., Tarchi, A., et al. 2005a, *Ap&SS*, 295, 107
 Henkel, C., Peck, A. B., Tarchi, A., et al. 2005b, *A&A*, 436, 75
 Hibbard, J. E., & van Gorkom, J. H. 1996, *AJ*, 111, 655
 Hofner, P., Baan, W. A., & Takano, S. 2006, *AJ*, 131, 2074
 Högbom, J. A. 1974, *A&AS*, 15, 417
 Honma, M., Yoon, K. C., Bushimata, T., et al. 2004, *PASJ*, 56, L15
 Hummel, E., & Jorsater, S. 1992, *A&A*, 261, 85
 Ishihara, Y., Nakai, N., Iyamoto, N., et al. 2001, *PASJ*, 53, 215
 Jaffe, D. T., Guesten, R., & Downes, D. 1981, *ApJ*, 250, 621
 Kondratko, P. T., Greenhill, L. J., Moran, J. M., et al. 2006, *ApJ*, 638, 100
 Kotilainen, J. K., Reunanen, J., Laine, S., & Ryder, S. D. 2001, *A&A*, 366, 439
 Krips, M., Eckart, A., Krichbaum, T. P., et al. 2007, *A&A*, 464, 553
 Krolik, J. H. 2001, *New Astron. Rev.*, 45, 625
 Laine, S., van der Marel, R. P., Rossa, J., et al. 2003, *AJ*, 126, 2717
 Liljeström, T., & Gwinn, C. R. 2000, *ApJ*, 534, 781
 Lo, K. Y. 2005, *ARA&A*, 43, 625
 Mauersberger, R., Wilson, T. L., & Henkel, C. 1988, *A&A*, 201, 123
 McDonald, A. R., Muxlow, T. W. B., Wills, K. A., Pedlar, A., & Beswick, R. J. 2002, *MNRAS*, 334, 912
 Miyoshi, M., Moran, J., Herrnstein, J., et al. 1995, *Nature*, 373, 127
 Morganti, R., Tsvetanov, Z. I., Gallimore, J., & Allen, M. G. 1999, *A&AS*, 137, 457

- Muxlow, T. W. B., Pedlar, A., Wilkinson, P. N., et al. 1994, *MNRAS*, 266, 455
- Neff, S. G., Ulvestad, J. S., & Teng, S. H. 2004, *ApJ*, 611, 186
- Neufeld, D. A., Maloney, P. R., & Conger, S. 1994, *ApJ*, 436, L127
- Ott, M., Witzel, A., Quirrenbach, A., et al. 1994, *A&A*, 284, 331
- Parra, R., Conway, J. E., Diamond, P. J., et al. 2007, *ApJ*, 659, 314
- Peck, A. B., Henkel, C., Ulvestad, J. S., et al. 2003, *ApJ*, 590, 149
- Read, A. M. 2005, *MNRAS*, 359, 455
- Simonetti, J. H., Diamond, P. J., Uphoff, J. A., Boboltz, D., & Dennison, B. 1993, in *Astrophysical Masers*, ed. A. W. Clegg, & G. E. Nedoluha, LNP, 311
- Stanford, S. A., & Balcells, M. 1990, *ApJ*, 355, 59
- Tarchi, A., Neininger, N., Greve, A., et al. 2000, *A&A*, 358, 95
- Tarchi, A., Henkel, C., Peck, A. B., & Menten, K. M. 2002a, *A&A*, 389, L39
- Tarchi, A., Henkel, C., Peck, A. B., & Menten, K. M. 2002b, *A&A*, 385, 1049
- Veilleux, S., Kim, D.-C., Sanders, D. B., Mazzarella, J. M., & Soifer, B. T. 1995, *ApJS*, 98, 171
- Veron-Cetty, M.-P., & Veron, P. 1986, *A&AS*, 66, 335
- Vlemmings, W. H. T., Bignall, H. E., & Diamond, P. J. 2007, *ApJ*, 656, 198
- Wills, K. A., Pedlar, A., & Muxlow, T. W. B. 1998, *MNRAS*, 298, 347
- Wu, Y.-F., Shi, J.-R., Wang, J.-Z., Jiang, D.-R., & Huang, X.-Y. 1999, *Chinese Astronomy and Astrophysics*, 23, 454
- Yun, M. S., & Hibbard, J. E. 2001, *ApJ*, 550, 104
- Zhang, J. S., Henkel, C., Kadler, M., et al. 2006, *A&A*, 450, 933